工學碩士學位論文

Detection of an anthrax biomarker by screen-printed fluorescent sensors

스크린 프린팅 기법으로 제조된 형광 센서를
이용한 탄저균의 검출

2013年 8月

서울大學校 大學院

化學生物工學部

李 仁 圭

Abstract

Detection of an anthrax biomarker by screen-printed fluorescent sensors

Inkyu Lee

School of Chemical and Biological Engineering

The Graduate School

Seoul National University

Since the 2001 anthrax attacks, efforts have focused on the development of an anthrax detector with rapid response and high selectivity and sensitivity. Here, we fabricated a fluorescence sensor by screen-printing method for detecting anthrax biomarker with high sensitivity and selectivity. A lanthanide–ethylenediamine tetraacetic acid complex was printed on a flexible polyethersulfone film. Screen-printing deposition of fluorescent

detecting moieties produced fluorescent patterns that acted as a visual alarm against anthrax.

List of Abbreviations

DPA: dipicolinic acid

EDTAD: ethylenediamine tetraacetic acid dianhydride

Eu: europium

FT-IR: Fourier transform-infrared

Ln: lanthanide

NMR: nuclear magentic resonance

PES: polyethersulfone

PVA: poly (vinyl alcohol)

Tb: terbium

List of Tables

List of Figures

Contents

Chapter 1. Introduction

1.1 Anthrax disease

Anthrax is caused by *Bacillus anthracis*, an encapsulated, gram-positive, spore-forming, rod-shaped bacterium. There are four types of anthrax: cutaneous anthrax, inhalational anthrax, gastrointestinal anthrax, and oropharyngeal anthrax. Cutaneous anthrax is the most common form and the oropharyngeal is the rarest form. Anthrax is primarily a disease of grazing animals such as cattle, sheep, horses, and goats. Inhalational anthrax is also known as Woolsorters' disease because people of this profession are more likely to contract anthrax [1].

Cutaneous anthrax represents over 95% of anthrax cases and results from direct contact with spores or the bacilli. The arms are most likely to be affected. The incubation period is typically less than a day. The initial clinical presentation is localized itching followed by a papular lesion that changes into vesicular. A black eschar develops within 7 to 10 days after the initial lesion. Treatment is ciprofloxacin 500 mg orally (PO) twice a day (bid) or doxycycline 100 mg PO bid. Therapy needs to be continued for 60 days. If neck involvement occurs then the intravenous route needs to be used for the

antibiotics.

Inhalational anthrax results from inhaling spores. The incubation period for inhalational anthrax is less than a week but in rare cases takes weeks. The initial symptoms include low-grade fever, nonproductive cough, malaise, fatigue, myalgias, and chest discomfort. Upper respiratory symptoms are rare. Rhonchi may be heard with a stethoscope. A relatively specific feature of anthrax seen on the chest X-ray is mediastinal widening. Hemorrhagic pleural effusions may also be seen with a radiograph. Subsequent symptoms occur 1 to 5 days after initial symptoms and presents with an abrupt onset of high fever and severe respiratory distress (dyspnea, stridor, cyanosis). Thereafter shock and death can occur within 24 to 36 hours. Specimens from the blood, pleural fluid and cerebral spinal fluid should be obtained. These specimens need to be obtained before initiating antimicrobial therapy but do not wait for cultures to come back prior to starting therapy. Death results when toxins from the bacteria spread throughout the body. Treatment consists of either ciprofloxacin intravenous 400 mg every (q) 12 hours or doxycycline 100 mg q 12 hours. An additional antibiotics should also be administered. Patients may be converted to PO antibiotics when clinically stable. Sixty days of treatment with antibiotics is required because of the presence of spores.

Gastrointestinal anthrax results from the consumption of undercooked or

raw meat or from dairy products from infected animals. The incubation period is 1 to 7 days. Initial symptoms include nausea, vomiting, anorexia, fever, hematemesis, and bloody diarrhea. Mesenteric adenopathy is likely to be seen on the computed tomography scan. After 2 to 4 days ascites develop. Shock and death occur with 2 to 5 days of onset. Samples of the blood and ascitic fluid are to be sent for cultures. Treatment is similar to inhalational anthrax. Oropharyngeal anthrax occurs within 1 to 7 days after expo-sure. Initial symptoms include fever, neck swelling (can be unilateral or bilateral), severe throat pain, dysphagia, and ulcers at the base of the tough. The subsequent phase includes the ulcers progressing to necrosis and an impaired airway from swelling. Cultures from the blood and throat need to be obtained. Treatment is similar to inhalational anthrax.

Anthrax meningitis is complication that can result from any form of anthrax. If meningitis is suspected, ciprofloxacin is preferred over doxycycline. The latter has poor penetration into the central nervous system. Seizures may result from the meningitis and are treated with anticonvulsants. *Bacillus anthracis* can go into a dormant phase by developing spores. The spores can survive in many environmental conditions for years. *Bacillus anthracis* exists in soil as spores and is found worldwide. The ability of anthrax to produce spores makes it attractive and useful as a bioweapon. The nonspecific initial symptoms of inhalational anthrax make it especially

dangerous. Person-to-person transmission of anthrax has not been reported but standard precautions need be followed with cutaneous anthrax. Natural occurring inhalational anthrax is so rare that any case should be presumed a biological attack until proven otherwise [1].

Anthrax is an acute disease and a potential biological warfare agent caused by *Bacillus anthracis*. Inhalation of 10^4 *B. anthracis* spores can result in death within 24–48 h. An anthrax sensor with rapid response and high selectivity and sensitivity is key to minimizing the impact of a bioterrorism event or outbreak [2,3]. *B. anthracis* spores are enclosed by protective layers, allowing the spores to survive harsh external conditions. A major component of the protective layers is dipicolinic acid (DPA), accounting for 5–15% of the dry mass of the spore [4–6]. Therefore, DPA can be used as a unique biomarker of *B. anthracis* [7].

1.2 Lanthanide luminescence

Complexes of Tb(III) and Eu(III) can in some cases be highly luminescent and typically exhibit emission lifetimes in the millisecond range. These long lifetimes provide a facile means to detect biomolecules labeled with lanthanide from the short-lived background emission of biosystems [8]. This strategy known as Time-Resolved Fluorescence has been commercially

exploited in the field of FlouroImmunoassay (TR-FIA). Lanthanide ions complexed to a variety of ligands have been developed, which permits the tuning of the emission wavelengths from 520 nm to 680 nm and life- times from 50 to 2,500 µs. Promising complexes of Tb(III) and Eu(III) for biological applications are abundant and some prominent, recent examples will be discussed here. Very simple ligands have been shown to greatly enhance the Tb(III) and Eu(III) emission upon complexation due to favourable energy transfer from the excited ligand's triplet state to the emissive levels of the ion.

These ligands, when provided with appropriate functional groups as precursors of covalent linkers to biomolecules, have been utilized for the labelling of the latter and proven useful as highly sensitive luminescent probes in immunoassays. The sturdy binding of these ligands to the lanthanide ions is evidenced by the strong emission displayed by the conjugated proteins in biological media.

The changes in the intensity of the Eu(III) luminescence upon binding to proteins and enzymes have been utilized to examine the ligation sphere within the active site, whereas distance and conformational information under physiological conditions has been obtained from energy transfer studies, either between two lanthanide ions or from the protein residues to Eu(III) or Tb(III) bound to the active site.

The sensitive detection of single-stranded regions of DNA, including mutations and mismatches, is critical in nucleic acid hybridization assays with applications scoping from the determination of genetic and infectious diseases to accurate personal identification. Luminescence enhancement of a given probe in the presence of nucleic acids or other targeted biomolecules can in principle yield such detection, with marked safety and environmental advantages over radioactive labelling.

The valence $4f$ electrons of trivalent lanthanide ions are well shielded from the environment by the outer core $5s$ and $5p$ electrons and are thus minimally involved in bonding. Because of this shielding, the atomic properties of these ions are typically retained after complexation. The total ligand-field splitting of an f-electron term is rarely more than a few hundred cm^{-1}, while for transition metal complexes, d-orbital splittings of 25,000 cm^{-1} are not uncommon. As a result of the small LF splitting for the Ln(III) complexes, radiationless decay processes are relatively inefficient and emission from these complexes is common. Therefore, the absorption and emission spectra of Ln(III) ions consist of sharp, narrow bands corresponding to the ff transitions of the metal ion. Figure 1 shows the most significant energy levels for several lanthanide ions. The ff transitions are Laporte forbidden, resulting in low molar absorption coefficients in the near-UV and visible ranges (<10 $M^{-1} \cdot cm^{-1}$) and long luminescence lifetimes in

the millisecond range. The number of observed bands depends on the particular lanthanide ion and its arrangement of electronic states.

Upon complexation with ligands, only minimal changes are observed in the electronic absorption and emission spectra, such as small displacements in the peak positions usually towards longer wavelengths and changes in the relative intensities of some of the emission peaks. Direct excitation with UV radiation into the Ln(III) *ff* transitions always leads to weak emission.

As mentioned before, emission from Ln(III) ions can often be quenched by high frequency vibrations of solvents or ligands such as those of OH, CH, or NH bonds. This undesired, efficient deactivation of lanthanide ion luminescence led to an intensive search for appropriate organic ligands to achieve the shielding of lanthanide ions from the solvent. As expected, in water and ethanol/methanol mixtures the lifetimes of the complexed Eu(III) ions were increased. But the excitation of the complexed lanthanide ion must also be achieved *via* the organic ligand which would thus act as an antenna or sensitizer, thereby compensating for the low absorption coefficient of the lanthanide ion. Hence, complexes with the proper organic chromophoric units displayed important enhancements, several orders of magnitude larger. In these cases the excitation of the ligand is followed by intramolecular energy transfer from the ligand triplet state to the sensitized lanthanide-based emission in com-plexes with the proper organic chromophoric units

displayed important enhancements, several orders of magnitude larger. In these cases the excitation of the ligand is followed by intramolecular energy transfer from the ligand triplet state to the lower-lying emissive lanthanide excited state (Figure 2) [8].
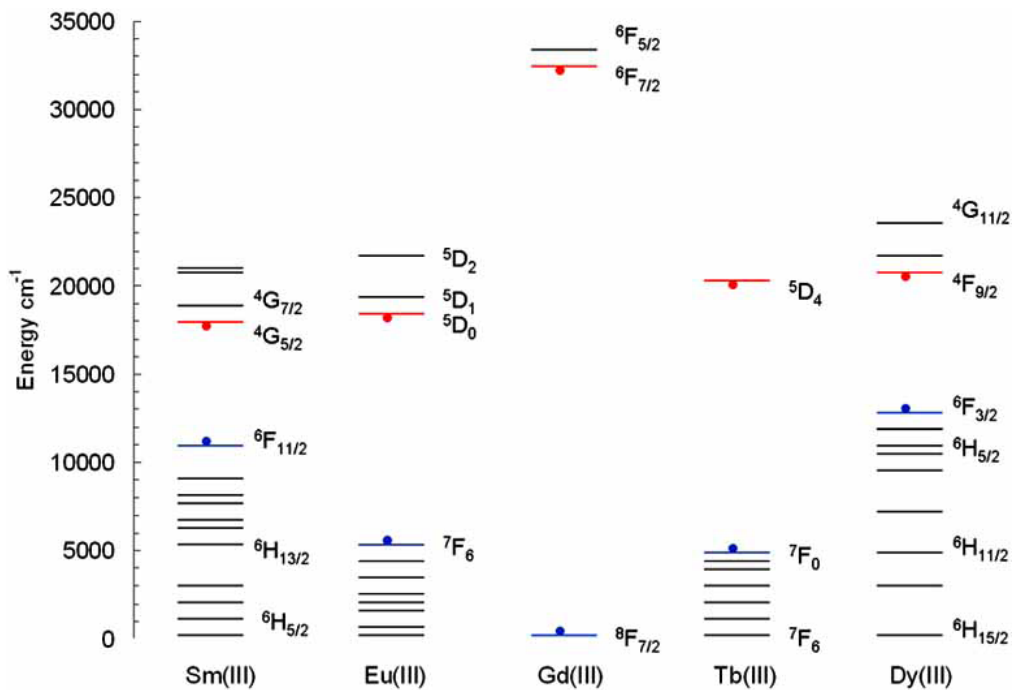
Figure 1. Important energy levels for several Ln(III) ions (Highest Occupied = above-dotted levels, Lowest Unoccupied = below-dotted levels) [8].
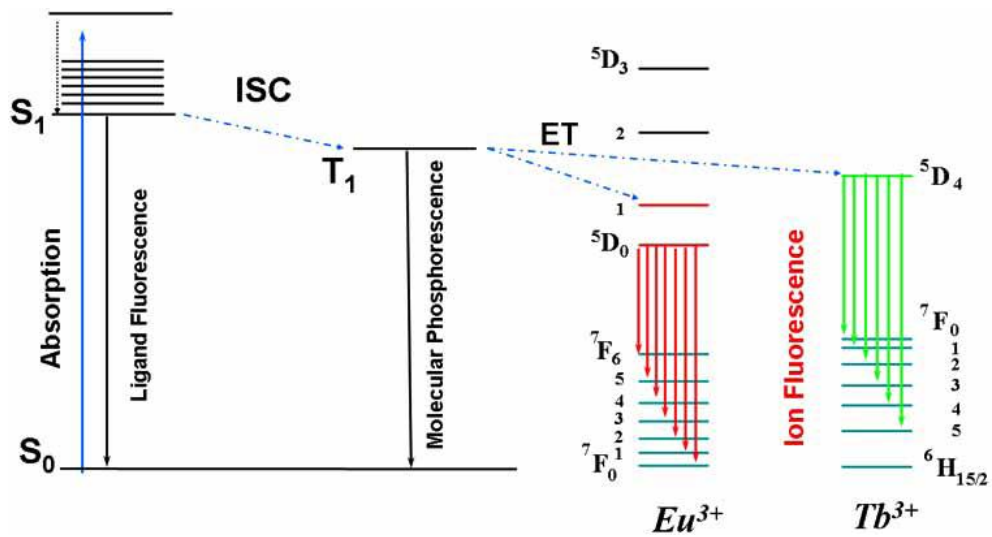
Figure 2. Jablonski diagram expliciting the energy transfer to the Eu(III) and
Tb(III) emissive levels [8].

1.3 Anthrax biomarker detection *via* lanthanide luminescence

Several methods have been applied for sensing anthrax, including polymerase chain reaction (PCR), immunoassays, surface-enhanced Raman spectroscopy, and lanthanide ion-based luminescence [7].

Vast amounts of work have been dedicated to the design of ligands containing nitrogenated heterocyclic rings for lanthanide complexation with the idea of exploiting their luminescent capabilities. Pyridine ring is the heterocycle most frequently employed in its combination with itself or with other rings for the luminescence sensitization of Eu(III) and Tb(III) chelates. One of the simplest ligands containing pyridine is DPA. Their lanthanide complexes have been extensively studied concerning their luminescence properties. This tridentate ligand is able to form tris structures corresponding to nine coordination sites.

The study of the nature of the charge transfer states in spectra of the lanthanide salts of DPA was undertaken as well as the luminescent properties and lifetimes in aqueous solutions influenced by synergic agents and surfactants. The comparative study of the luminescent properties of Eu(III) and Tb(III) coordinated with DPA and thenoyltrifluoroacetone led to the conclusion that the lanthanide ion luminescence sensitized by the coordination with organic ligands depended on several factors, including the

11

number of atoms available from the ligand for coordination and the composition of the chelate. Some of these salts could be considered as fragments or experimental models of the lanthanide luminescence centers in lanthanide salts of parvalbumin or in helicates.

The luminescent properties of Eu(III) and Tb(III) coordinated with DPA in aqueous solution were studied, leading to the observation that the energy transfer process is less efficient with terbium than with europium. The aqueous solutions of the chelates Eu(III) and Tb(III) tris(DPA) have been shown to be convenient secondary standards for the determination of quantum yields of lanthanide complexes containing these ions. Although easy-to-handle buffered solutions displayed a constant quantum yield within a reasonably large range of concentration, their quantum yield was strongly pH-dependent.

Among applications of lanthanide complexes with the DPA ligand, that with Tb(III) was used for the bacterial endospore detection and determination (CaDPA is present in the endospore casing and is released into solution with $TbCl_3$). The 4-substituted derivatives of DPA are also effective energy donors for Tb(III) and Eu(III) ions. The complex between 4-iodoacetamidodipicolinic acid and Tb(III) was proposed for the labeling of protein molecules in luminescence immunoassays. The spectral properties of Tb(III) complexes with a series of 4-substituted analogues of DPA were

compared and the emission intensities followed the order of substituents: NH_2 > NHAc > OH > H > Cl ≈ Br while relative quantum yields of energy transfer kept to a slightly different order: NH_2 > OH > NHAc > Cl > H ≈ Br.

The DPA ligand has also been employed for ultratrace determination of selected lanthanides, especially Tb(III) and Eu(III). A surfactant, sodium dodecyl sulfate, was added to the solution to enhance the luminescence intensity of many lanthanide-ligand complexes by segregating the complex from quenchers and to achieve very low limits of detection.

The luminescence of lanthanides sensitized by meas of DPA and other ligands containing pyridine rings in organic and inorganic materials as mesoporous silica and sol-gels has been investigated. Even simple, unsubstituted bipyridine showed important enhancement of the optical properties of lanthanide-doped materials derived from zirconium phosphate. This behavior indicated that the ligand remained somewhat associated with the lanthanide incorporated into the material. Both the red ($^5D_0 \rightarrow ^7F_2$) and green ($^5D_4 \rightarrow ^7F_5$) fluorescence of Eu(III) and Tb(III), respectively, were enhanced within the studied solid matrices suggesting promising applications of these luminescent new materials [8].

Lanthanide ions readily bond with DPA in aqueous solution. Furthermore, lanthanide ion-based luminescence using elements such as europium and terbium has received attention due to unique properties, including narrow

13

emission bands, large Stokes shift, and long fluorescence lifetime [9]. These properties allow detection of anthrax with excellent sensitivity [10]. However, lanthanide ion-based detection has several drawbacks, including nonselective binding with other aromatic ligands, nonradiative quenching due to coordination with water, and false negatives due to interruption by anions. To overcome these problems, macrocycle coordination has been used to inhibit water binding with lanthanide ions [11].

1.4 Lanthanide-macrocycle complex

Although the method is rapid and straightforward, we aim to improve the Ln-DPA assay for detection of bacterial sporesand expand our understanding of the chemistry underpinning this sensor system. The potential for false positives or false negatives through complexation of anionic interferents to the trivalent terbium cation is a serious concern when the method is applied to environmental samples. Previous studies indicate that phosphate in particular can inhibit DPA binding or decrease,luminescence intensity. Further, coordinated water molecules,can quench Ln^{3+} luminescence by nearly an order of magnitude,,due to nonradiative deactivation from vibronic coupling of the OH oscillators with the excited lanthanide.

To eliminate water from the Tb^{3+}-coordination sphere and reduce the

potential for interfering ion effects, we have introduced the macrocyclic ligand to form a first generation DPA receptor site. The macrocyclic ligand meets our initial conditions for a receptor site ligand, in that it binds strongly to Ln^{3+} without impeding DPA binding. The extraordinary stability of the Ln(macrocycle)(DPA)⁻ complex has improved lanthanide-based detection of dipicolinate under optimal conditions. [5]

Macrocycles such as ethylenediamine tetraacetic acid dianhydride (EDTAD) and 1,4,7,10-tetraazacyclododecane-1,7-diacetate occupy six lanthanide coordination sites in aqueous solution, leaving three adjacent sites, which are occupied by water, available for DPA coordination [11]. Lanthanide–macrocycle complexes prevent the coordination of water molecules after DPA binding, thus providing selective DPA sensing.

1.5 Screen-printing method

Sensing *via* microarrays on a flexible substrate allows fast and real-time detection of multiple analytes [12,13]. Flexible sensors can be used in numerous applications, but the development of fabrication techniques remains challenging [14–16]. The screen-printing technique provides rapid, reproducible, and economic production of microarray sensors [17].

The first developments of screen printing date back to the beginning of

the 20 th century. It is a very versatile printing technique that allows for full 2-dimensional patterning of the printed layer. It is parsimonious and there is essentially no loss of coating solution during printing. Its main distinction from all other printing and coating techniques is a large wet film thickness and are quirement for are latively high viscosity and a low volatility of the coating solution. The pattern is obtained by filling the screen with an emulsion that is impervious to the coating solution in the areas where no print should appear. The area of the printed pattern is kept open (without emulsion). The screen is then filled with coating solution and brought into proximity of the substrate.

A so-called squeegee is forced into to screen bringing it into contact with the substrate and then drawn linearly across the screen thus forcing coating solution through the open areas onto the substrate and in that manner reproducing the pattern. Screen printing is currently used extensively in industry for simple tasks such as printing text an detch resistsand for complex task such as printing conductors for flexible electronics and keypads. It has also been reported used in the context of polymer so larcells in a few in stances. The large wet thickness, the requirement for a high viscosity and low volatility, has probably been a limiting factor, thus, so far the most suited polymer for printing is MEHPPV that has a suitable rheology (high viscosity at low concentration).

In the latter case the challenges of large wet thickness, viscosity and volatility were efficiently solved. Screen-printing is in herently batch operated but highly R2R compatible as exemplified on a Klemm line where rectangular screens are used and the material is passed through the machine at constant speed. The screen and support follow the web at constant speed while printing is in progress. After each print the screen and support reverses back and the printing cycle is repeated [18].

Screen-printing deposition of fluorescent sensing moieties offers direct visualization of fluorescent patterns due to binding with analytes. The screen-printing method has been applied to textiles and printed electronics, but fluorescence sensors based on screen-printing deposition have rarely been reported.

Here, we report fluorescence sensors for detecting anthrax with high sensitivity and selectivity. The anthrax detectors were prepared by screen-printing deposition on a polyethersulfone (PES) film. Printed lanthanide–macrocycle Eu(EDTA) and Tb(EDTA) complexes having well-defined shapes were fabricated through non-covalent binding.

Chapter 2. Experimental Details

2.1. Materials

The following chemicals were purchased and used as received: 2,6-pyridinedicarboxylic acid (DPA; Aldrich), 2,3-pyridine dicarboxylic acid (Aldrich), 2,5-pyridinedicarboxylic acid (Aldrich), 2-picolinic acid (Aldrich), 3,5-pyridinedicarboxylic acid (Aldrich), benzoic acid (Aldrich), isophthalic acid (Aldrich), nicotinic acid (Aldrich), terephthalic acid (Aldrich), dipicolinic acid (Aldrich), ethylenediamine tetraacetic acid dianhydride (EDTAD; Aldrich), polyvinyl alcohol (Aldrich), europium chloride (EuCl$_3$; Aldrich), and terbium chloride (TbCl$_3$; Aldrich). Polyethersulfone film (PES film) was purchased from PANAC Ltd. (Tokyo, Japan).

2.2. Preparation of ink pastes for screen-printing

The lanthanide-based ink pastes were prepared for screen-printing. To synthesize Eu(EDTA) paste, 2 mM EDTAD were reacted with the distilled water, and then, 2 mM EuCl$_3$ were added into the resulting ink paste. In the case of Tb(EDTA) paste, EDTAD (2 mM) and TbCl$_3$ (2 mM) were reacted

with the distilled water. To control the viscosity of the ink paste, polyvinyl alcohol (PVA; 8 wt%) was mixed with solution, and resulting mixture was dissolved by sonication for 3 h at 50 $^{\circ}$C.

2.3. Lanthanide-based anthrax detectors *via* screen-printing

To prepare lanthanide-based anthrax detector, pastes were coated on the PES film by screen-printing method (Screen-printer; SM-S320, SUNMECHANIX). Screen printing was performed at a scraper speed of 450 mm/s, squeege pressure of 500 kPa, and a squeeze speed of 450 mm/s using the print mode. After printing, the detector was dried for 4 h at 80 $^{\circ}$C. A Bomem MB 100 Fourier transform infrared (FTIR) spectrometer was used to characterize screen-printed Eu(EDTA), Tb(EDTA), Eu(EDTA)(DPA) and Tb(EDTA)(DPA) on PES film.

2.4. Quantum yield

Fluorescence quantum yield of lanthanide-based anthrax detector was calculated by a comparision method of the fluorescence emission with the standard reference, DAPI (Molecular Probes Inc.), in aqueous solution. The

fluorescence quantum yield of lanthanide-based anthrax detector was determined by following formula:

$$\Phi_{\text{L}} = \frac{F_{\text{L}}}{A_{\text{L}}} \times \frac{A_{\text{D}}}{F_{\text{D}}} \times \Phi_{\text{D}}$$

where Φ is the fluorescence quantum yield, F is the integrated emission intensities, and A is the absorption coefficient (at the relevant excitation wavelength). The suffix L means the term for lanthanide-based anthrax detector and D indicates the DAPI dye [19]. Under UV irradiation, both Eu(EDTA)(DPA) and Tb(EDTA)(DPA) showed intersecting point with DAPI at 330 nm. To calculate the quantum yield of sensors, the emission spectra of DAPI, Eu(EDTA) and Tb(EDTA) were excited at 330 nm.

2.5. DPA detection

All fluorescence spectra were measured on a JASCO FP-6500 spectrofluorometer. The fluorescence intensity changes were observed with increasing the concentration of $EuCl_3$ and $TbCl_3$, and the fluorescence intensity changes of the Eu(EDTA) were monitored at 616 nm ($\lambda_{\text{ex}} = 270$ nm) in the presence of DPA (0–1000 nM). In the case of Tb(EDTA)(DPA), the

fluorescence was measured at 545 nm (λ_{ex} = 250 nm).

Chapter 3. Results and Discussion

3.1 Fabrication of screen-printed anthrax biomarker detectors

Lanthanide-based fluorescence anthrax sensors (europium and terbium) were prepared *via* screen-printing deposition, as shown in Figure 3. Briefly, EDTAD and $EuCl_3$/$TbCl_3$ were inserted in a solution containing PVA. After reaction with EDTAD and $EuCl_3$/$TbCl_3$, the resulting pastes were converted into Eu(EDTA) and Tb(EDTA) complexes, respectively, and coated onto PES film by screen printing. ^{1}H-NMR peak shifts can verify the formation of the complex between the lanthanides and the EDTA (Figure 4~6). The EDTAD shows two peaks at 3.941 and 3.526 ppm, arising from the acetate–methylene protons and the backbone–methylene protons, respectively. The spectrum of Eu(EDTA) complex shows two peaks at 4.093 and 3.441 ppm, arising from the acetate–methylene protons and the backbone–methylene protons. The peaks at 4.310 and 3.537 ppm arose from the acetate–methylene protons and the backbone–methylene protons of Tb(EDTA) complex. The ratio of the two peak areas (2:1) in all 1H-NMR data is in agreement with the

theoretical ratio. There are peak shifts in the obtained 1H-NMR data of the lanthanide-EDTA complexes compared to the EDTAD. The chemical shifts of the proton signals in EDTA-complex are different from only EDTAD, therefore, the 1H-NMR results showed that lanthanide formed complex with EDTA very well. The lanthanide-macrocycle complexes help to maximize the positive surface area of the lanthanide ion binding site, which allows for better compatibility with the negative surface of the DPA. It is known that lanthanide-macrocycle platform has the high binding constants with DPA ($>10^9$ M^{-1}) [11], therefore, using lanthanide-macrocycle platform can result in highly sensitive detection of anthrax biomarker.

PES film was used because it is flexible and transparent. Screen printing can be applied to most solid surfaces, and the viscosity of the printing ink is critical to the screen-printing process [20]. PVA was added to increase the viscosity of the ink. In this experiment, 8 wt% PVA was added to maintain the printing shapes.

Figure 7a shows photographs of anthrax detectors printed on PES film. The screen-printing speed was 450 mm/s, and the standard printing cycle was less than 3 s, which is advantageous for mass production of anthrax detectors. Eu- and Tb-based anthrax detectors exhibited red emission at 616 nm and green emission at 545 nm, respectively, under 365-nm UV irradiation (Figure 7b, c). Red and green emissions were visible to the naked eye at low

concentrations of DPA (1000 nM), making this approach well suited for practical applications. DPA binding triggers strong luminescence that is facilitated by an absorption-energy transfer-emission process [21]. Flexibility is one of the advantages of the evaluated anthrax biomarker detector. We can obtain the flexible anthrax biomarker detector by screen-printing on the flexible polymeric substrates as shown in Figure 7d. This screen-printed anthrax biomarker detector also possesses stability and reproducibility. Even after 3 months later, the synthesized PES film maintains the Tb(EDTA) patterns without any leakage (Figure 8).
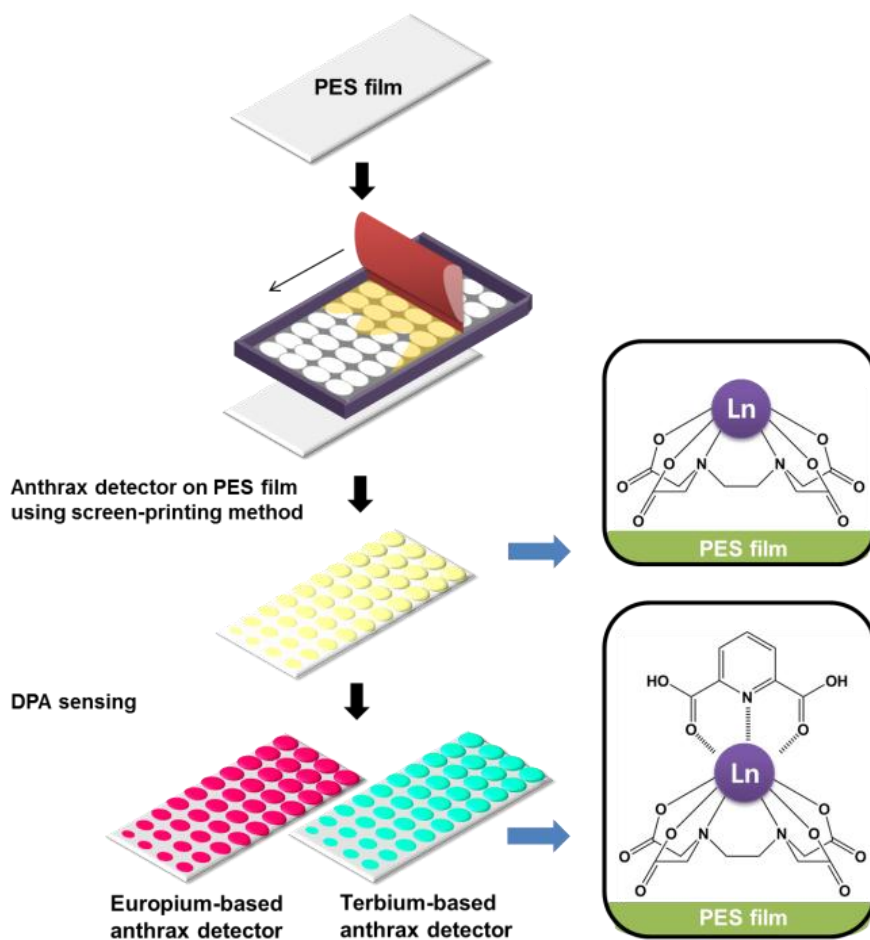
Figure 3. Schematic diagram of fabrication of lanthanide-based anthrax detectors using screen-printing method. The process was performed under optimized condition at a scraper speed of 450 mm/s, squeege pressure of 500 kPa, and a squeeze speed of 450 mm/s.
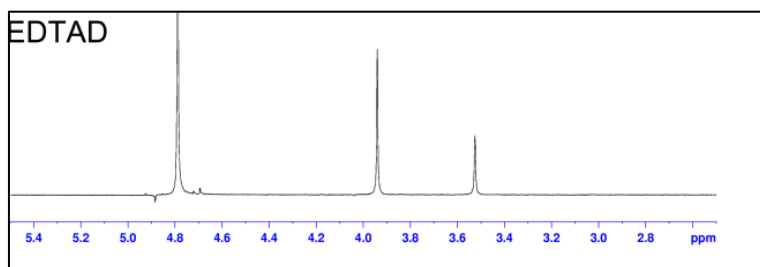
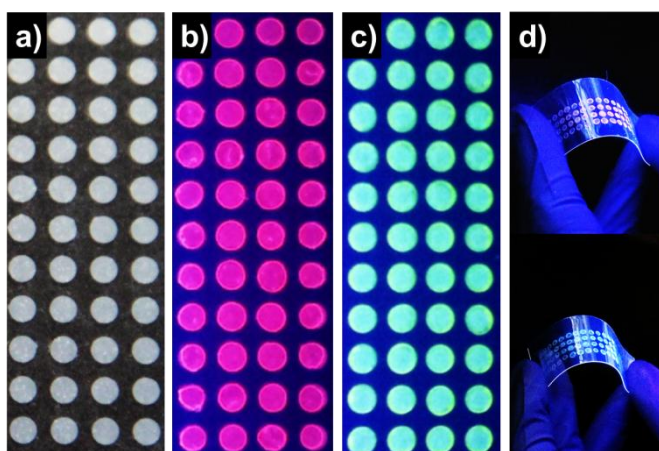**Figure 4.** The ^{1}H-NMR spectra of EDTAD in D_2O solvent
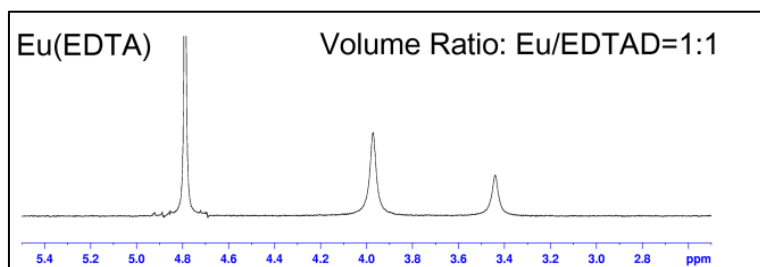
Figure 5. The ^{1}H-NMR spectra of the Eu(EDTA) complex in D_2O solvent
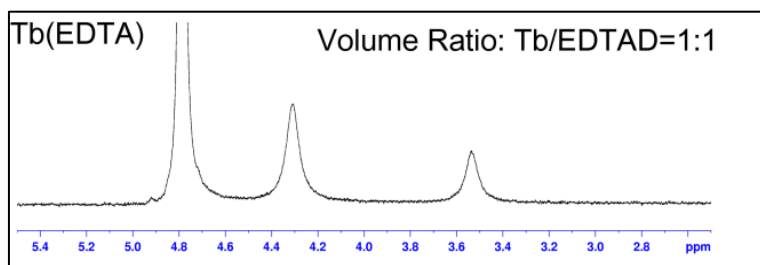
Figure 6. The ^{1}H-NMR spectra of the Tb(EDTA) complex in D_2O solvent

Figure 7. Photographs of a) pristine Eu-based anthrax detector, b) Eu-based anthrax detector in presence of DPA, c) Tb-based anthrax dectector in presence of DPA and d) bent sensors. (Diameter = 2 mm) The 1000 nM DPA solution was dropped onto the surface of sensory strips until dried. The image of fluorescent sensors was obtained under excitation with UV-lamp (λ_{ex}=254 nm).
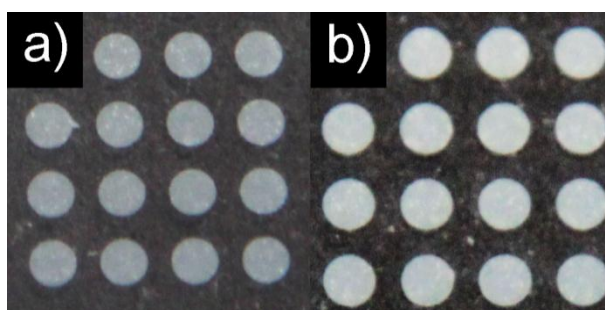
**Figure 8.** Photographs of Tb-based anthrax detector on PES film manufactured a) 3 months ago and b) recently.

3.2 Characterization of anthrax biomarker detectors

The formation of Eu(EDTA), Eu(EDTA)(DPA), Tb(EDTA), and Tb(EDTA)(DPA) on PES films was characterized by Fourier transform infrared (FTIR) spectroscopy (Figure 9, 10). The FTIR spectra of Eu-based anthrax detector and Tb-based anthrax detector show characteristic peaks of metal–EDTA complexes, including the C=O stretching band at 1655 cm^{-1}, the C–H(CH$_2$) stretching band at 1430 cm^{-1}, and the COO$^-$ stretching bands at 1375 and 1334 cm^{-1} [22]. These peaks indicate the successful screen printing of Eu(EDTA) and Tb(EDTA) pastes on PES film. In the spectra of Eu(EDTA)(DPA) and Tb(EDTA)(DPA) on screen-printed anthrax detectors, the C=O stretching band at 1714 cm^{-1}, pyridine ring stretching band at 1440–1410 cm^{-1}, and C–H rocking band at 720 cm^{-1} were assigned to DPA [23]. The FTIR peak assignments are summarized in Table 1. These results indicate that the surfaces of the lanthanide-based anthrax detectors were successfully modified with DPA.
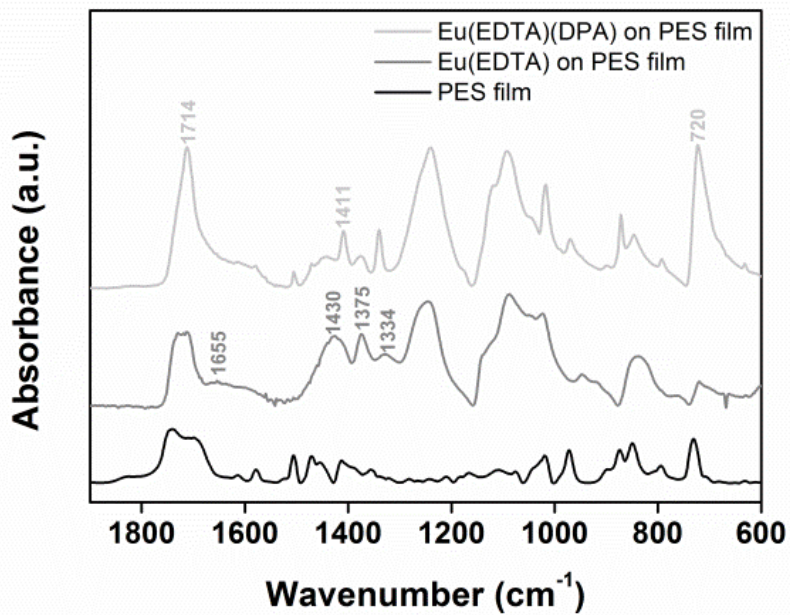
Figure 9. FTIR spectra of Eu-based anthrax detector before reaction with DPA and after reaction with DPA(DPA=1000 nM).
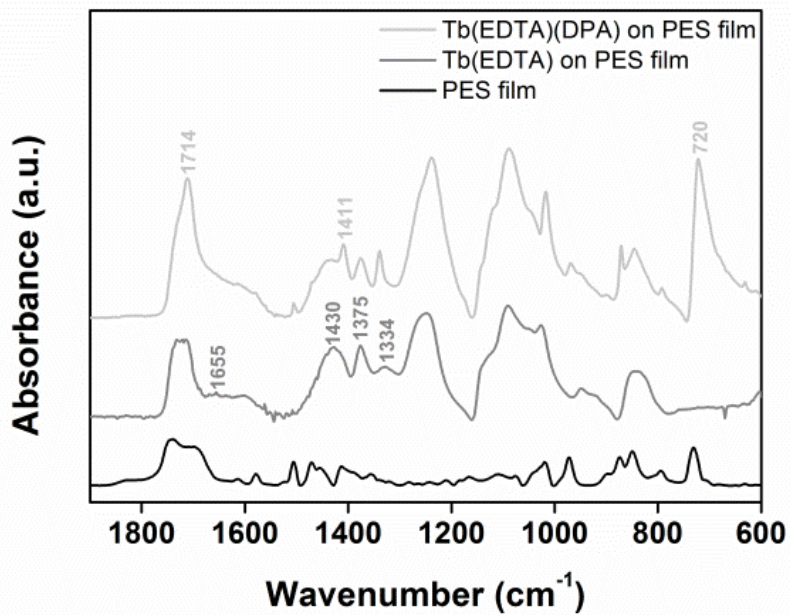
Figure 10. FTIR spectra of Tb-based anthrax detector before reaction with DPA and after reaction with DPA (DPA=1000 nM).

Table 1. FTIR assignments of Ln(EDTA) and Ln(EDTA)(DPA) complex.

| Materials	Wavenumber[a]	Assignments
Ln(EDTA) complex	1655	C=O stretching
	1430	C–H(CH$_2$) stretching
	1375, 1344	COO$^-$ stretching
Ln(EDTA)(DPA) complex	1714	C=O stretching
	1440-1410	Pyridine ring stretching
	720	C–H rocking

[a] unit: cm^{-1}

3.3 Optimal concentration of lanthanide metals

To determine the optimal concentration of lanthanide metals, the fluorescence intensities of the screen-printed anthrax detectors were plotted against the concentrations of $EuCl_3$ and $TbCl_3$ (Figure 11, 12). The fluorescence of lanthanide-based anthrax detectors using screen-printing method was most intense when 2 mM of $EuCl_3$ and 2 mM of $TbCl_3$ were added to the solution. The maximum fluorescence intensity was observed when lanthanide metals and EDTAD reacted in a 1:1 molar ratio. Nonradiative quenching from water coordination in $[Ln(DPA) \cdot (H_2O)_6]^+$ decreases the overall quantum yield and sensitivity [11]. Lanthanide–macrocycle complexes maximize the positive surface area of Ln^{3+} binding sites through addition of macrocycle amine hydrogens, which have high affinity for the negative surface of DPA [24].
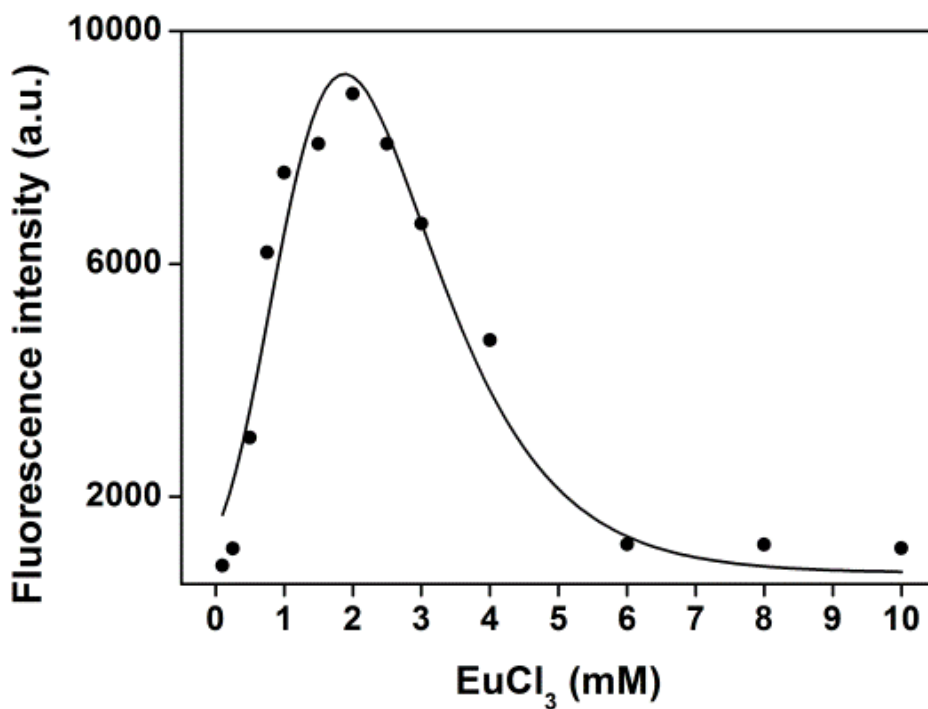
Figure 11. Fluorescence intensity plot of anthrax detector containing 2mM of EDTAD with changing the concentration of $EuCl_3$ in presence of 1000 nM DPA. The fluorescence intensity of the Eu-based anthrax detector were monitored at 616 nm (λ_{ex} = 270 nm).
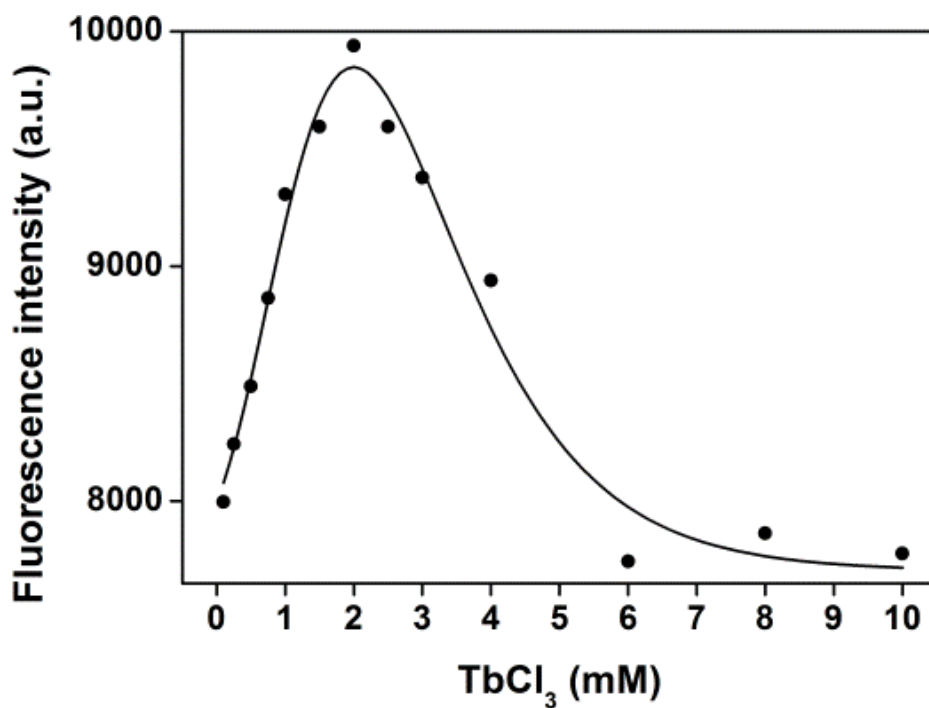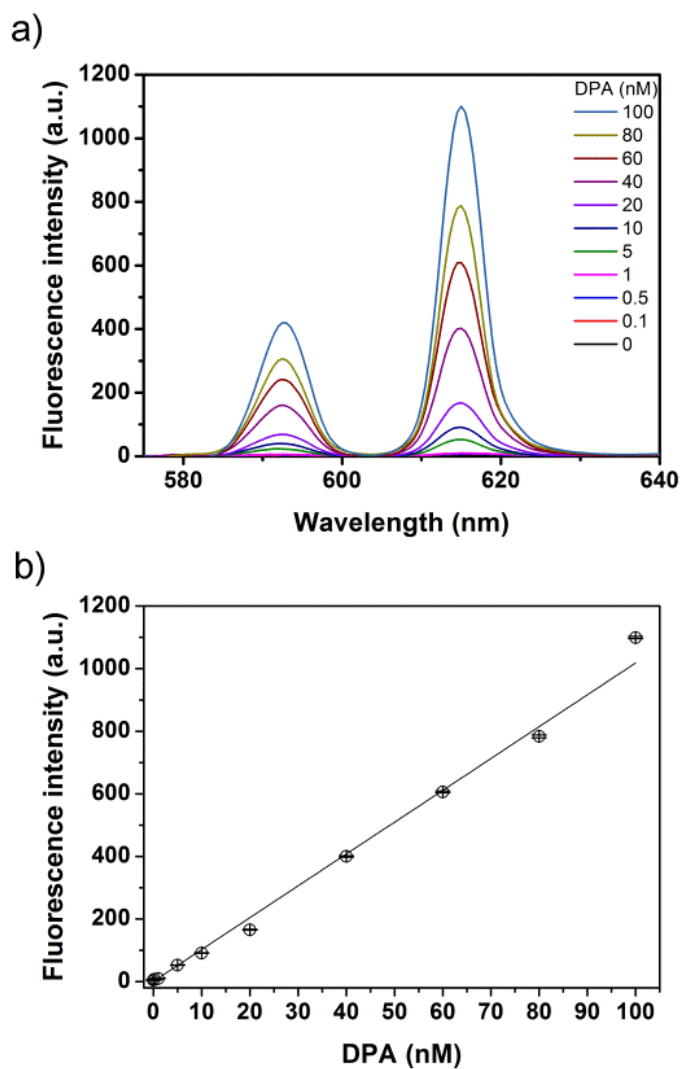
Figure 12. Fluorescence intensity plot of anthrax detector containing 2mM of EDTAD with changing the concentration of $TbCl_3$ in presence of 1000 nM DPA. The fluorescence intensity of the Eu-based anthrax detector were monitored at 545 nm (λ_{ex} = 250 nm).

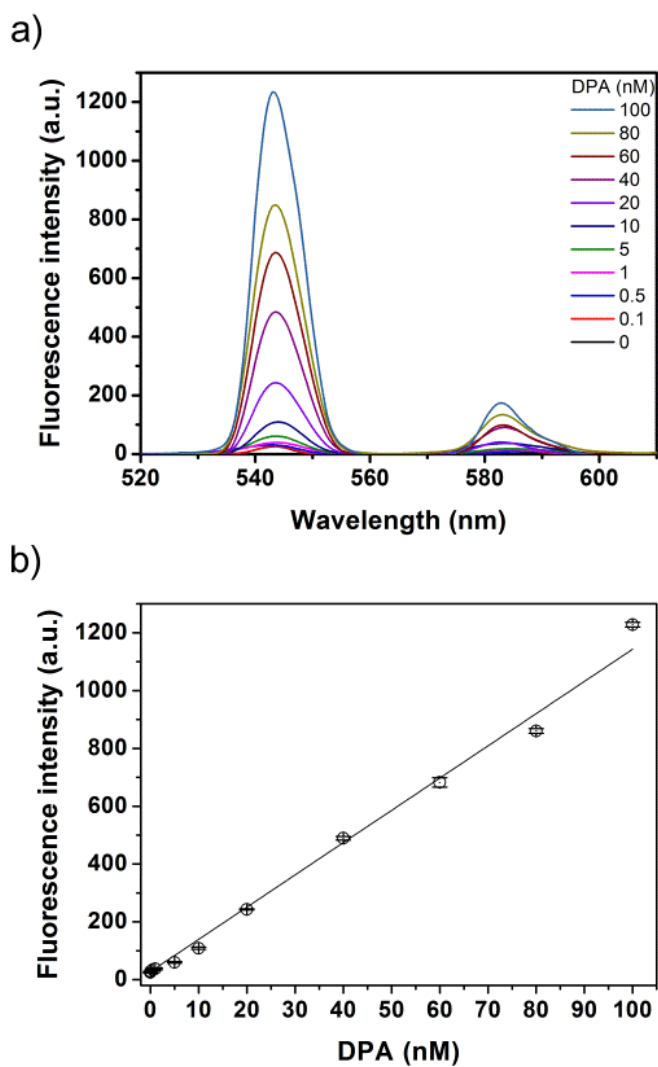## 3.4 Sensitivity of screen-printed anthrax biomarker detectors

To evaluate the sensitivity of screen-printed anthrax detectors, various concentrations of DPA were added to Eu-based anthrax detector and Tb-based anthrax detector. The fluorescence intensities of Eu(EDTA) complex on Eu-based anthrax detector and Tb(EDTA) complex on Tb-based anthrax detector increased with increasing concentration of DPA and were highly sensitive to DPA (Figure 13, 14). The anthrax detectors showed a linear correlation between the emission intensities at 616 and 545 nm and the concentration of DPA (adjusted R^2 = 0.992 and 0.991 for Eu(EDTA) and Tb(EDTA), respectively). The limit of detection (LOD) values for DPA *via* binding with Eu(EDTA) complex on Eu-based anthrax detector and Tb(EDTA) complex on Tb-based anthrax detector were 0.5 nM and 0.1 nM, respectively. The LOD value is established at a signal to noise of 3. Upon addition of DPA, two sharp emission peaks appeared at 593 and 616 nm due to formation of the Eu(EDTA)(DPA) complex *via* transition of the Eu^{3+} excited states $^5D_0 \rightarrow {}^7F_J$ (J = 0, 1, and 2) [8]. Binding of DPA reduced the nonradiative quenching of Eu^{3+} emission, resulting in an increase in the quantum yield and a corresponding reinforcement of the detection sensitivity. The sensitive $^5D_0 \rightarrow {}^7F_2$ change resulted in large changes in the Eu^{3+} center and the displacement of three coordinating water molecules from the Eu^{3+}

center. The sensitivity of Tb-based anthrax detector was 1.2-fold higher than Eu-based anthrax detector because of the small energy gap and corresponding strong coupling between the DPA triplet state and the $^5D_4$ excited state of terbium [25]. The fluorescence quantum yield of Eu(EDTA)(DPA) on Eu-based anthrax detector was *ca*. 0.78 (red line; excitation at 270 nm) and that of Tb(EDTA)(DPA) on Tb-based anthrax detector was *ca*. 0.68 (green line; excitation at 250 nm). Moreover, the whole sensing procedure took 80 s, enabling the rapid detection of anthrax (Figure 15, 16). The rapid detection of DPA *via* film-type anthrax detector has advantage in rapid response to inhalation of *B.anthracis,* which can result in death within 24-48 h [2].

Figure 13. (a) Fluorescence spectra of Eu-based anthrax detector in presence of DPA with concentration dependence. The fluorescence intensity were monitored at 616 nm (λ_{ex} = 270 nm). (b) The linear correlation between the emission intensity at 616 nm and the concentration of DPA.

Figure 14. (a) Fluorescence spectra of Tb-based anthrax detector in presence of DPA with concentration dependence. The fluorescence intensity were monitored at 545nm (λ_{ex} = 250 nm). (b) The linear correlation between the emission intensity at 545 nm and the concentration of DPA.
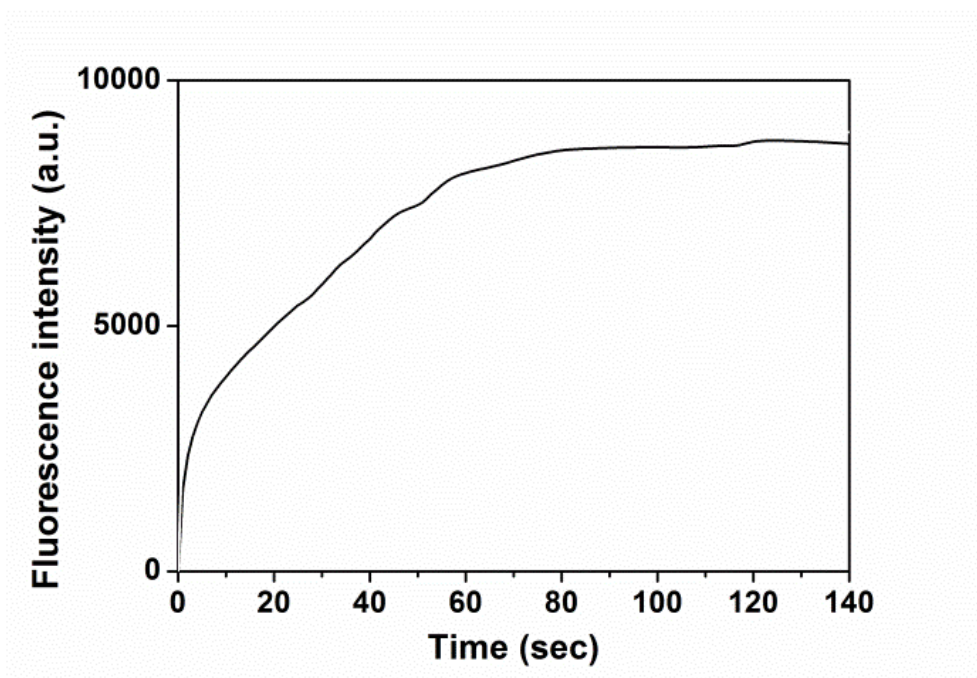
Figure 15. Time-dependent fluorescence intensity plot of Eu-based anthrax detector after DPA insertion (1000 nM; detected at 616 nm emission).
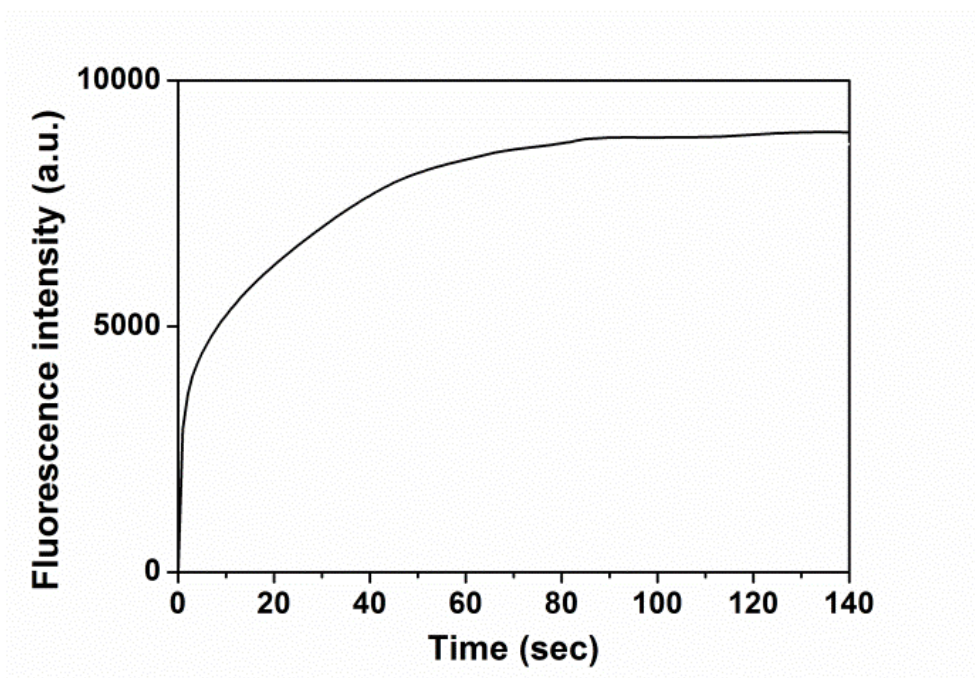
Figure 16. Time-dependent fluorescence intensity plot of Tb-based anthrax detector after DPA insertion (1000 nM; detected at 545 emission).

3.5 Selectivity of screen-printed anthrax biomarker detectors

To determine the selectivity of Eu-based anthrax detector and Tb-based anthrax detector against other competitive aromatic ligands, the detectors were reacted with nine aromatic ligands (1000 nM each): 2,3-pyridinedicarboxylic acid, 2,5-pyridinedicarboxylic acid, 2-picolinic acid, 3,5-pyridinedicarboxylic acid, benzoic acid, isophthalic acid, nicotinic acid, terephthalic acid, and DPA (Figure 17). Table 2 summarizes the normalized fluorescence intensity ratios (I/I_0) of lanthanide-based anthrax detectors against aromatic ligands. DPA binding to Eu(EDTA) and Tb(EDTA) complexes on evaluated anthrax detectors resulted in noticeable fluorescence enhancement (>100 fold) compared with other aromatic ligands; almost no change in fluorescence intensity was observed for the other aromatic ligands.. These results confirm that screen-printed fluorescence sensors for anthrax detection have the ability to enhance fluorescence due to DPA interactions with Eu(EDTA)(DPA) and Tb(EDTA)(DPA) with high sensitivity and selectivity, thereby enabling accurate sensing for practical applications. Additionally, the screen-printed anthrax biomarker detectors have a potential to detect anthrax biomarker in vapor phase. We investigated the fluorescence intensity of the screen-printed anthrax biomarker detectors under 1000 nM DPA in vapor phase in the vacuun oven (Figure 18, 19). The results showed

that the screen-printed anthrax biomarker detectors also have the ability to detect the DPA in vapor phase not only in water solution.
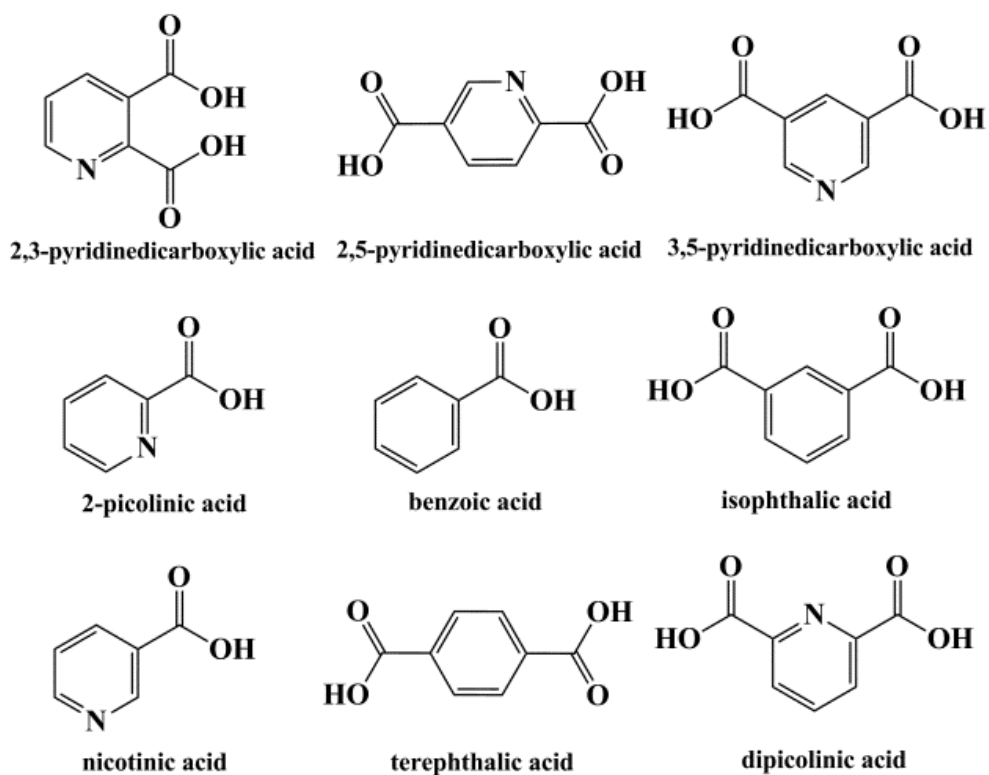
Figure 17. The structure of aromatic ligands used in this study: 2,3-pyridinedicarboxylic acid, 2,5-pyridinedicarboxylic acid, 2-picolinic acid, 3,5-pyridinedicarboxylic acid, benzoic acid, isophthalic acid, nicotinic acid, terephthalic acid and dipicolinic acid (DPA).

Table 2. Normalized fluorescence intensity (I/I_0) changes upon addition of DPA and different aromatic ligands onto Eu-based anthrax detector and Tb-based anthrax detector (1000 nM for each ligand).

Aromatic ligands	Eu-based anthrax detector	Tb-based anthrax detector
	(I/I_0-1)	(I/I_0-1)
DPA	270.16	219.62
2,3-pyridinedicarboxylic acid	2.91	0.86
2,5-pyridinedicarboxylic acid	7.43	3.13
2-picolinic acid	4.98	-0.41
3,5-Pyridinedicarboxylic acid	0.42	0.68
Benzoic acid	0.35	-0.18
Isophthalic acid	-0.54	0.36
Nicotinic acid	1.27	2.47
Terephthalic acid	0.21	-0.16
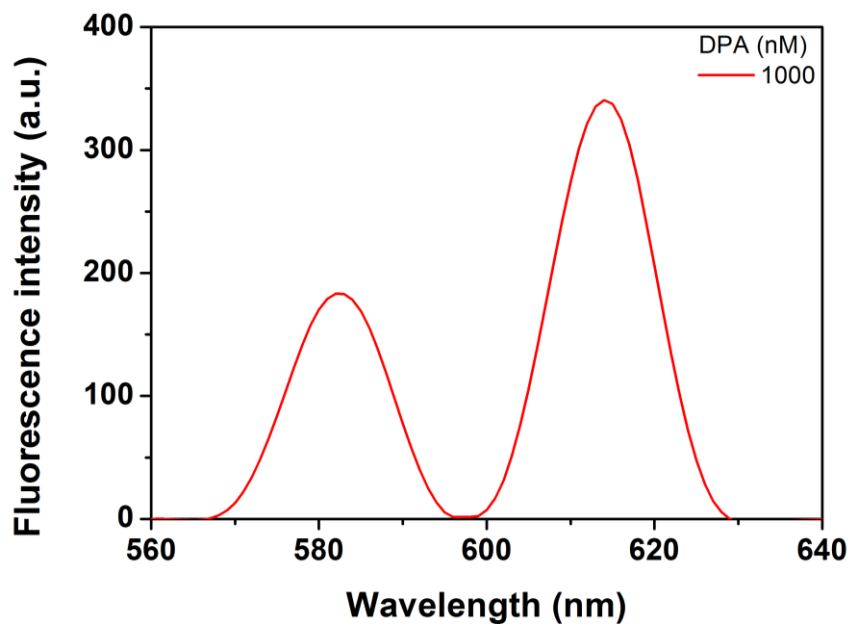
Figure 18. Fluorescence spectra of Eu-based anthrax detector in presence of 1000 nM DPA in the vapor phase. The fluorescence intensity were monitored at 616 nm (λ_{ex} = 270 nm).
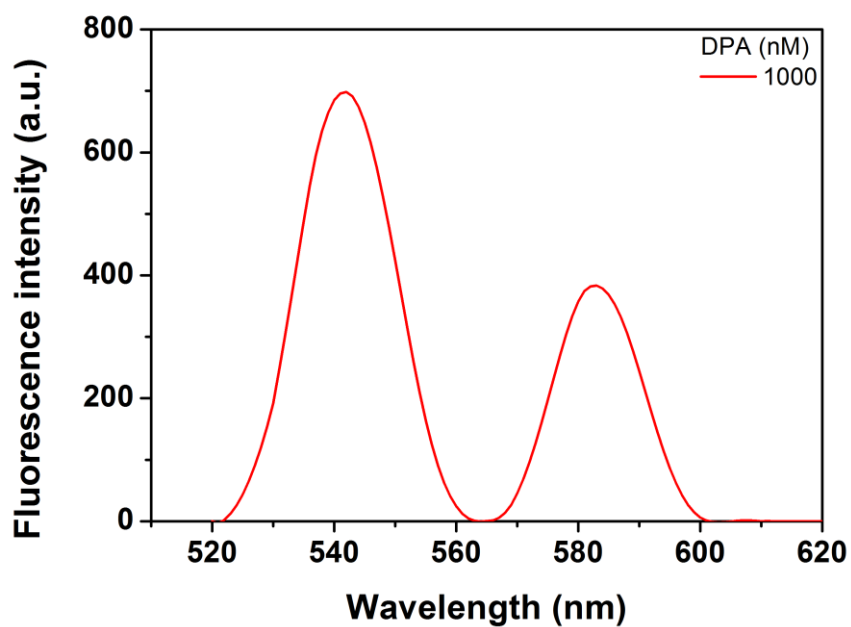
Figure 19. Fluorescence spectra of Tb-based anthrax detector in presence of 1000 nM DPA in the vapor phase. The fluorescence intensity were monitored at 545 nm (λ_{ex} = 250 nm).

Chapter 4. Conclusion

Lanthanide-based fluorescent sensors for anthrax detection were prepared by a screen-printing method. We could obtain the flexible anthrax biomarker detectors by screen-printing on the flexible PES film. Additionally, The screen-printed Eu(EDTA) and Tb(EDTA) complexes enabled highly sensitive and selective sensing of DPA. The lanthanide-based anthrax biomarker detectors could contribute to the development of DPA sensors.

References

[1] P. D. Anderson, PharmD and G. Bokor, *J. Pharm. Pract*. **2012**, *25*, 521.

[2] W.K. Oh, Y.S. Jeong, J. Song, J. Jang, *Biosens. Bioelectron.* **2011,** *29*, 172.

[3] S.M. Lev, G. Gasparich, F. Choi, L. King, J. Moore, S. Zimmerman, *Talanta* **2011,** *85*, 1734.

[4] B. Eker, M.D. Yilmaz, S. Schlautmann, J.G.E. Gardeniers, J. Huskens, *Int. J. Mol. Sci.* **2011,** *12*, 7335.

[5] M.L. Cable, J.P. Kirby, D.J. Levine, M.J. Manary, H.B. Gray, A. Ponce, *J. Am. Chem. Soc.* **2009**, *131*, 9562.

[6] K. Ai, B. Zhang, L. Lu, *Angew. Chem. Int. Ed*. **2009,** *48*, 304.

[7] M.D. Yilmaz, S.H. Hsu, D.N. Reinhoudt, A.H. Velders, J. Huskens, *Angew. Chem. Int. Ed.* **2010**, *49*, 5938.

[8] E. Brunet, O. Juanes, J.C. Rodriguez-Ubis, *Curr. Chem. Biol*. **2007,** *1*, 11.

[9] K.M.L. Taylor, W. Lin, *J. Mater. Chem.* **2009**, *19*, 6418.

[10] W.J. Rieter, K.M.L. Taylor, W. Lin, *J. Am. Chem. Soc.* **2007**, *129*, 9852.

[11] M.L. Cable, J.P. Kirby, K. Sorasaenee, H.B. Gray, A. Ponce, *J. Am. Chem. Soc.* **2007**, *129*, 1474.

[12] F.J. Rawson, W.M. Purcell, J. Xu, R.M. Pemberton, P.R. Fielden, N. Biddle, J.P. Hart, *Talanta* **2009***, 77,* 1149.

[13] R.-H. Peng, R.-R. Xu, X.-Y. Fu, A.-S. Xiong, W. Zhao, Y.-S. Tian, B. Zhu, X.-F. Jin, C. Chen, H.-J. Han, Q.-H. Yao, *J. Hazard. Mater.* **2011**, *189*,

19.

[14] O.S. Kwon, S.J. Park, J.S. Lee, E. Park, T. Kim, H.W. Park, S.A. You, H. Yoon, J. Jang, *Nano Lett.* **2012,** *12*, 2797.

[15] S. Ma, R. Li, C. Lv, W. Xu, X. Gou, *J. Hazard. Mater*. **2011**, *192*, 730.

[16] J.-M. Kim, S.K. Jha, D.-H. Lee, R. Chand, J.-H. Jeun, Y.-S. Kim, *J. Ind. Eng. Chem.* **2012,** *18,* 1642.

[17] L.L. Qu, D.W. Li, J.Q. Xue, W.L. Zhai, J.S. Fossey, Y.T. Long, *Lab. Chip.* **2012,** *12,* 876.

[18] F. C. Krebs, *Sol. Energy mater. Sol. Cells* **2009,** *93*, 394

[19] C. Wu, J. McNeill*, Langmuir* **2008,** *24,* 5855.

[20] W. Yin, D.H. Lee, J. Choi, C. Park, S.M. Cho, *Korean J. Chem. Eng*. **2008,** *25*, 1358.

[21] J.P. Kirby, M.L. Cable, D.J. Levine, H.B. Gray, A. Ponce, *Anal. Chem.* **2008.** *80*, 5750.

[22] S. Pasieczna-Patkowska, J. Ryczkowski, *Eur. Phys. J. Spec. Top.* **2008,** *154,* 351.

[23] K. McCann, J. Laane, *J. Mol. Struct.* **2008,** *890,* 346.

[24] A. Zhang, M. Lü, Z. Qiu, Y. Zhou, Q. Ma, *Mater. Chem. Phys.* **2008,** *109,* 105.

[25] X. Zhang, L. Chi, S. Ji, Y. Wu, P. Song, K. Han, H. Guo, T.D. James, J. Zhao, *J. Am. Chem. Soc.* **2009,** *131,* 17452.

초　　록

　　스크린 프린팅 기법과 두 개의 란탄족 이온을 이용해 제조된 형광 센서의 탄저균 검출을 대표적인 탄저균 바이오마커인 디피콜린산을 이용해 알아보았다. 두 종류의 서로 다른 란탄족 이온(유로피움 그리고 터비움)을 에틸렌디아민 사초산과 수용액 상태에서 결합시키고 폴리비닐알코올을 넣어 점도를 높인 후 폴리에터술폰 필름 위로 스크린 프린팅을 수행하였다. 란탄족 이온과 에틸렌디아민 사초산과의 결합은 핵자기공명 분광법과 푸리에 변환 적외분광법을 이용해 관찰했다. 란탄족 이온의 최적 농도 측정과 제조된 형광 센서의 디피콜린산 비율 측정은 자외선 등과 형광분석기를 통해 체계적으로 조사되었다. 유로피움을 이용한 형광 센서와 터비움을 이용한 형광 센서 모두 놀라운 검출 한계 (각각 0.5 나노몰, 0.1 나노몰)를 보여주었으며 터비움을 이용한 형광 센서가 보다 높은 감도를 보여주었다. 이는 작은 에너지 갭과 디피콜린산 삼중 상태와 들뜬 상태의 터비움 사이의 강결합에 의한 것이라 사료된다. 추가적으로 유로피움과 터비움을 사용한 두 형광 센서의 다양한 방향족 리간드의 검출 능력을

53

비교해보았을 때 디피콜린산에 대해서 뛰어난 선택성(각각 135배, 200배)을 나타내었다. 이러한 결과들은 스크린 프린팅 방법과 두 종류의 란탄족 이온이 함께 탄저균 검출에 이용되었을 때 높은 검출 감도와 선택적 검출에 대한 중요한 정보들을 제공하게 될 것으로 판단된다.